

Subtropical Pacific SST Variability Related to the Local Hadley Circulation during the Premature Stage of ENSO

Yoshimitsu CHIKAMOTO

Center for Climate System Research, University of Tokyo, Kashiwa, Japan

Youichi TANIMOTO

Faculty of Environmental Earth Science, Hokkaido University, Sapporo, Japan

Hitoshi MUKOUGAWA

Disaster Prevention Research Institute, Kyoto University, Kyoto, Japan

and

Masahide KIMOTO

Center for Climate System Research, University of Tokyo, Kashiwa, Japan

(Manuscript received 9 April 2009, in final form 4 January 2010)

Abstract

Formation processes of negative (positive) sea surface temperature anomalies (SSTAs) in the subtropical North and South Pacific associated with the ENSO warm (cold) events are examined using reanalysis and in-situ observational datasets. During the premature stage of the ENSO warm events, negative SSTAs appear over the subtropical North Pacific in the February–March period and over the subtropical South Pacific after April, and vice versa in the ENSO cold events. One month prior to the formation of these subtropical negative SSTAs, the negative air humidity anomaly and anomalous downward motion appear at the same location in either the Northern or Southern hemisphere. Associated with these atmospheric anomalies, the strengthened descending branch of local Hadley circulation is observed during the January–February period in the Northern hemisphere and after March in the Southern hemisphere, which coincides with the seasonal transition of the climatological local Hadley circulation from the Northern to Southern hemisphere. Our linear decomposition analysis of surface heat flux anomalies indicates that the negative air humidity anomaly, as well as anomalies in wind speed, contributes to the formation of the subtropical negative SSTAs through the enhanced latent heat flux induced by the anomalous air–sea humidity difference. These results suggest that the anomalous downward motion associated with the changes in local Hadley circulation can induce the subtropical negative SSTAs through the surface humidity variability. A possible mechanism for the subtropical air–sea interaction associated with the local Hadley circulation is discussed.

Corresponding author: Yoshimitsu Chikamoto, Center for Climate System Research, University of Tokyo 5-1-5, Kashiwanoha, Kashiwa, Chiba, 277-8568, Japan.
E-mail: chika44@ccsr.u-tokyo.ac.jp
© 2010, Meteorological Society of Japan

1. Introduction

The well-known feature of the subtropical Pacific sea surface temperature anomaly (SSTA) during the El Niño and the Southern Oscillation (ENSO)

warm events is a horse shoe like structure of cold SST encompassing the tongue-like structure of warm SST in the eastern equatorial Pacific and vice versa in the cold events (e.g., Rasmusson and Carpenter 1982; Trenberth et al. 1998; Wallace et al. 1998; Larkin and Harrison 2002; Alexander et al. 2004). This subtropical SST variability shows the seasonal evolution associated with the development of equatorial SSTAs during the ENSO event. Figure 1 shows the composite difference maps of seasonal SSTAs between the ENSO warm and cold events (the definitions of the ENSO warm and cold events are described in Section 2). During the January-February-March (JFM) period in the premature stage of the ENSO events, negative SSTAs are observed west of 150°W in the subtropical

North Pacific from 15°N to 30°N, while such significant anomalies are not apparent in the subtropical South Pacific (Fig. 1a). In the subtropical North Pacific, the negative SSTAs become prominent at the center of 165°W during the April-May-June (AMJ) period (Fig. 1b), and move further north of 35°N in the following July-August-September (JAS) period (Fig. 1c). In the subtropical South Pacific, on the other hand, negative SSTAs begin to emerge over the region east of Australia, extending from the equator to 40°S and tilting southeastward during the April-May-June (AMJ) period, three months later than in the subtropical North Pacific and persist until the mature stage of the ENSO event with their area extending eastwards (Fig. 1d).

In association with the ENSO events, the SSTAs

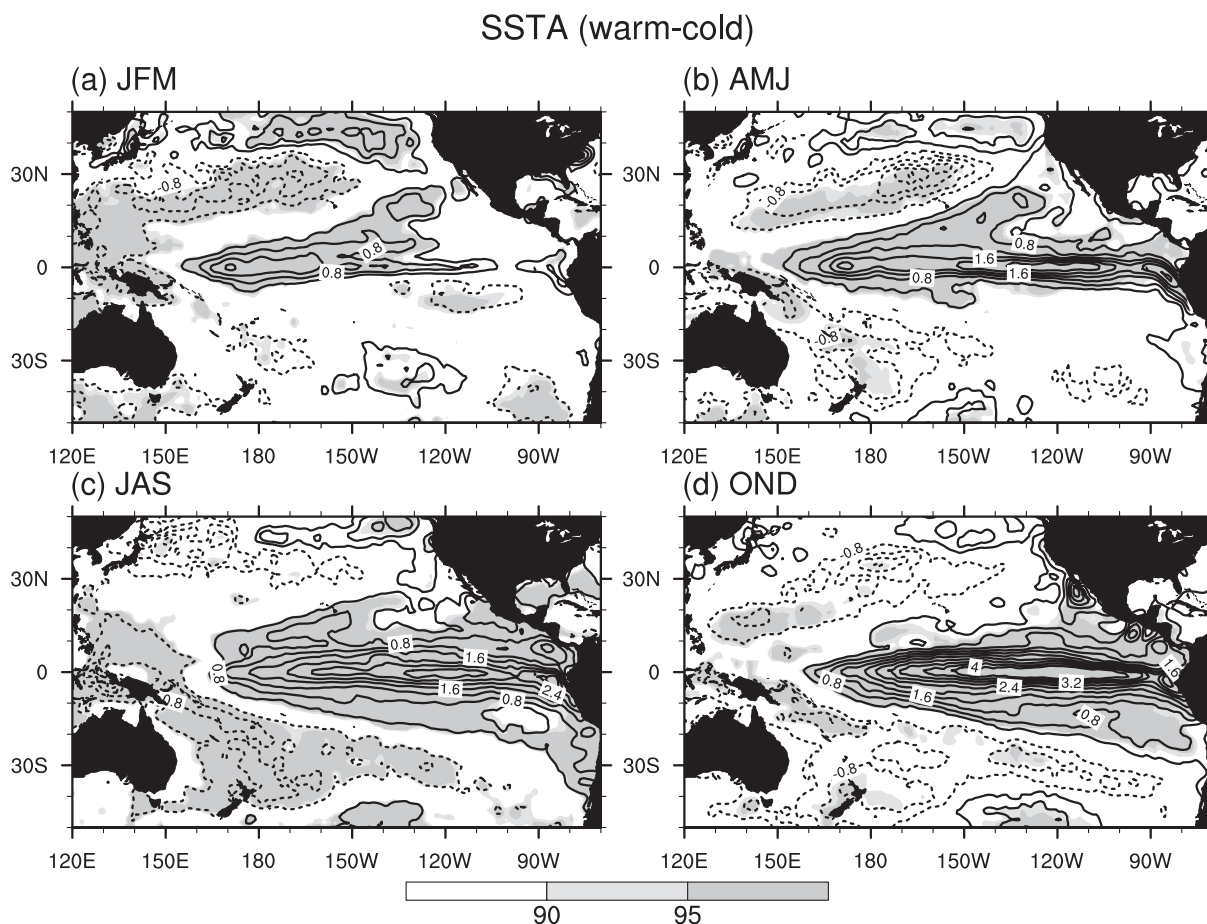


Fig. 1. Composite difference maps of SSTAs in (a) January-February-March, (b) April-May-June, (c) July-August-September, and (d) October-November-December periods of the five warm and three cold events of ENSO. The contour interval is 0.4 K. Zero contours are omitted. Anomalies exceeding the thresholds for significance at the 90% and 95% levels are indicated by light and dark shaded regions, respectively.

in the equatorial Pacific affect atmospheric meridional circulations via changes in precipitation and upward motion over the central and western tropical Pacific. Oort and Yienge (1996) indicate that the Hadley circulation, calculated from the zonal mean streamfunction by using the zonal mean meridional wind component, is strengthened in both hemispheres during the ENSO warm events. Wang (2002), by analyzing the regional meridional circulation, shows that the strengthened local Hadley circulation is observed in the western North Pacific during the November–January period, one year before the mature stage of the ENSO warm events. The strengthened Hadley circulation induced by the ENSO forcing may affect humidity variations in the lower atmosphere and thereby produce the subtropical SST variability through a change in sea surface evaporation, because the descending branch of local Hadley circulation induces a dry condition in the lower atmosphere by vertical moisture advection and surface moisture flux divergence (Sun and Lindzen 1993; Sun and Oort 1995; Sohn et al. 2001; Kawamura et al. 2002; Yoneyama 2003). Chikamoto and Tanimoto (2005) showed that a latent heat flux anomaly induced by an air–surface humidity anomaly is the major factor to form a local SST anomaly in the Caribbean region after the mature stage of the ENSO events. These studies suggest that the air–surface humidity variability under the descending branch of the Hadley circulation over the subtropical Pacific is important to induce the local SST variability during the ENSO events. Weng (2009) also implied the existence of atmospheric forced subtropical SST variability on the basis of a statistical mode obtained from the time-mode extended singular value decomposition analysis between the upper ocean heat content and SST anomalies.

Recent studies focus on the roles of the subtropical SST variability in the phase transition and amplification of the ENSO events. Wang and Zhang (2002) pointed out that off-equatorial, cool SSTA maintains anomalous Philippine Sea anti-cyclone through a positive thermodynamic feedback (Wang et al. 2000). The resultant surface easterlies over the equatorial region can excite a cold Kelvin wave, which is indispensable for the phase transition of the ENSO events (Kug and Kang 2006; Ohba and Ueda 2007). Another role of the subtropical SST variability is the link between extratropical and tropical oceans (Liu et al. 1994; McCreary and Lu 1994; Gu and Philander 1997). Shin and Liu (2000)

showed that thermocline anomalies in the midlatitudes can efficiently penetrate into the equator. On the basis of the results of these studies, Sun et al. (2004) demonstrated that enhanced ocean cooling in the subtropical Pacific results in a regime with stronger ENSO activity. Thus, the subtropical SSTAs may feed back to the ENSO cycle and/or modulate the amplitude of ENSO.

In the present study, we examine how the subtropical negative (positive) SSTAs associated with the variations in the local Hadley circulation are produced during the premature stage of the ENSO warm (cold) event. Since the changes in the local Hadley circulation will accompany surface air humidity variability, we show the formation process of air humidity anomaly associated with the seasonal cycles of the local Hadley circulation. This air humidity variability is key to understanding the air–sea interaction over subtropical regions.

The rest of this paper is organized as follows. Section 2 describes the datasets and defines the ENSO warm and cold events from the Niño3 index. In Section 3, we examine the interannual variability of air–surface humidity related to the descending branch of local Hadley circulation. In Section 4, we analyze the formation processes of the subtropical SSTAs induced by the air humidity variability. On the basis of the results from our analyses, we discuss a possible mechanism to induce the air humidity variation and suggest an atmospheric positive feedback in Section 5. The results are summarized in Section 6.

2. Datasets

To capture the ENSO-related variability in the tropical Pacific, monthly horizontal wind, vertical p -velocity, and specific humidity fields at eight pressure levels are obtained from the National Centers for Environmental Prediction–Department of Energy Atmospheric Model Intercomparison Project-II Reanalysis (NCEP2; Kanamitsu et al. 2002) data on a $2.5^\circ \times 2.5^\circ$ grid. Monthly latent and sensible heat fluxes from the ocean surface (upward positive), surface longwave and shortwave radiation fluxes, zonal and meridional wind components at 10-m height, and specific humidity at 2-m height are also taken from the NCEP2 approximately on a $1.875^\circ \times 1.875^\circ$ Gaussian grid. Monthly SST data are obtained from the National Oceanic and Atmospheric Administration optimum interpolation SST version 2 (OISST; Reynolds et al. 2002) on a $1^\circ \times 1^\circ$ grid. To calculate monthly latent heat flux

components, we used surface flux variables of surface wind speed at 10-m height, saturation specific humidity at the ocean surface, and air–sea humidity difference in specific humidity between the ocean surface and at a 2-m height on the Gaussian grid. The surface wind speed at a 10-m height is derived from 4 times daily of zonal and meridional wind components at 10-m height in the NCEP2 data. From the linearly interpolated SST and surface pressure, the monthly saturation specific humidity at the ocean surface and the air–sea differences in specific humidity between the ocean surface and at 2-m height are calculated on the Gaussian grid.

The surface latent heat fluxes of the reanalysis data are less reliable than other elements in the free atmosphere due to insufficient treatments of the planetary boundary layer (Trenberth and Guillemot 1995; Trenberth and Guillemot 1998). Therefore, we employ the $2^\circ \times 2^\circ$ monthly dataset of surface latent heat fluxes based on individual marine meteorological reports archived in the Comprehensive Ocean–Atmosphere Data Set (COADS; Woodruff et al. 1987). This dataset contains some missing values in the equatorial and South Pacific regions since satellite observations and spatial interpolation were not used. Details of the calculation procedure are described in Tanimoto and Xie (2002) and Tanimoto et al. (2003). We calculate the monthly climatological means based on a 21- or 22-year period from December 1981 to December 2002 for NCEP2 and OISST datasets and for a 46-year period from January 1950 to December 1995 for COADS. The monthly anomalies are defined as departures from the climatological mean values.

To represent the magnitude of the ENSO warm and cold events, we extract eight warm (cold) years of 1957/58, 65/66, 72/73, 82/83, 87/88, 91/92, 94/95, and 97/98 (1955/56, 67/68, 70/71, 73/74, 75/76, 84/85, 88/89, and 99/00) from the SSTAs in the Niño3 region, as described in Chikamoto and Tanimoto (2006), which is defined as the averaged monthly SSTAs from November through January in the following year (exceeding one standard deviation). Hence, we take the warm (cold) events of 7 (7) years in COADS and of 5 (3) years in NCEP2 and OISST. We analyze composite difference maps between the ENSO warm and cold events, hereafter simply referred to as composite in the ENSO warm event. The anomalies with the opposite polarity are observed in the ENSO cold event. In the COADS datasets, composites calculated from more than four events are employed.

3. Subtropical air humidity variability during the premature stage of the ENSO events

As we stated in the introduction, the subtropical SSTAs during the premature stage of the ENSO event have a different time evolution between the North and South Pacific. In Fig. 2, we have a closer look at the monthly evolution of the SSTAs from January to April during the premature stage of the ENSO event. In January, negative SSTAs lower than -0.5°C appear in the subtropical North Pacific near the date line. These negative SSTAs become prominent in February (Fig. 2b) and are zonally elongated along 25°N in the following March. In contrast, a coherent structure of negative SSTA is not so apparent in the subtropical South Pacific during this period (Figs. 2b,c). In April, the prominent negative SSTAs exceeding 1.0°C begin to emerge in the subtropical South Pacific (Fig. 2d) and maintain their anomalies until the mature stage of the ENSO event (Figs. 1b–d).

To examine the temporal evolution of surface air humidity anomalies related to the SSTA formation over the subtropical Pacific, we drew monthly composite maps of specific humidity anomaly at a 2-m height (q'_a) and surface wind anomalies from January to April (Fig. 3). In the subtropical North Pacific, significant negative q'_a lower than -1.0 g kg^{-1} associated with northerly wind anomalies is observed near the date line in January (Fig. 3a) and extends in the westward direction along 25°N in February (Fig. 3b). In the following March and April, the local maximum of negative q'_a in the subtropical North Pacific gradually decreases its amplitude (Figs. 3c,d). Instead, significant negative q'_a and southerly wind anomalies emerge in the subtropical South Pacific during this period.

Figure 4 shows the temporal evolution of the specific humidity anomaly at a 2-m height (q'_a) and the saturation specific humidity anomaly at the sea surface (q_o^{*l}) averaged over the subtropical North Pacific (160°E – 170°W , 20°N – 40°N) and the subtropical South Pacific (160°E – 170°W , 20°S – 40°S). Note that q_o^{*l} is a function of the local SSTA. As shown in Fig. 4, negative q'_a , much lower than q_o^{*l} , is formed over the subtropical North Pacific in January and February before the mature stage of the ENSO events. This anomalous air–sea difference in specific humidity indicates that the negative air humidity anomalies contribute to form negative SSTAs in the subtropical North Pacific, as will be shown in the next section. After March, however,

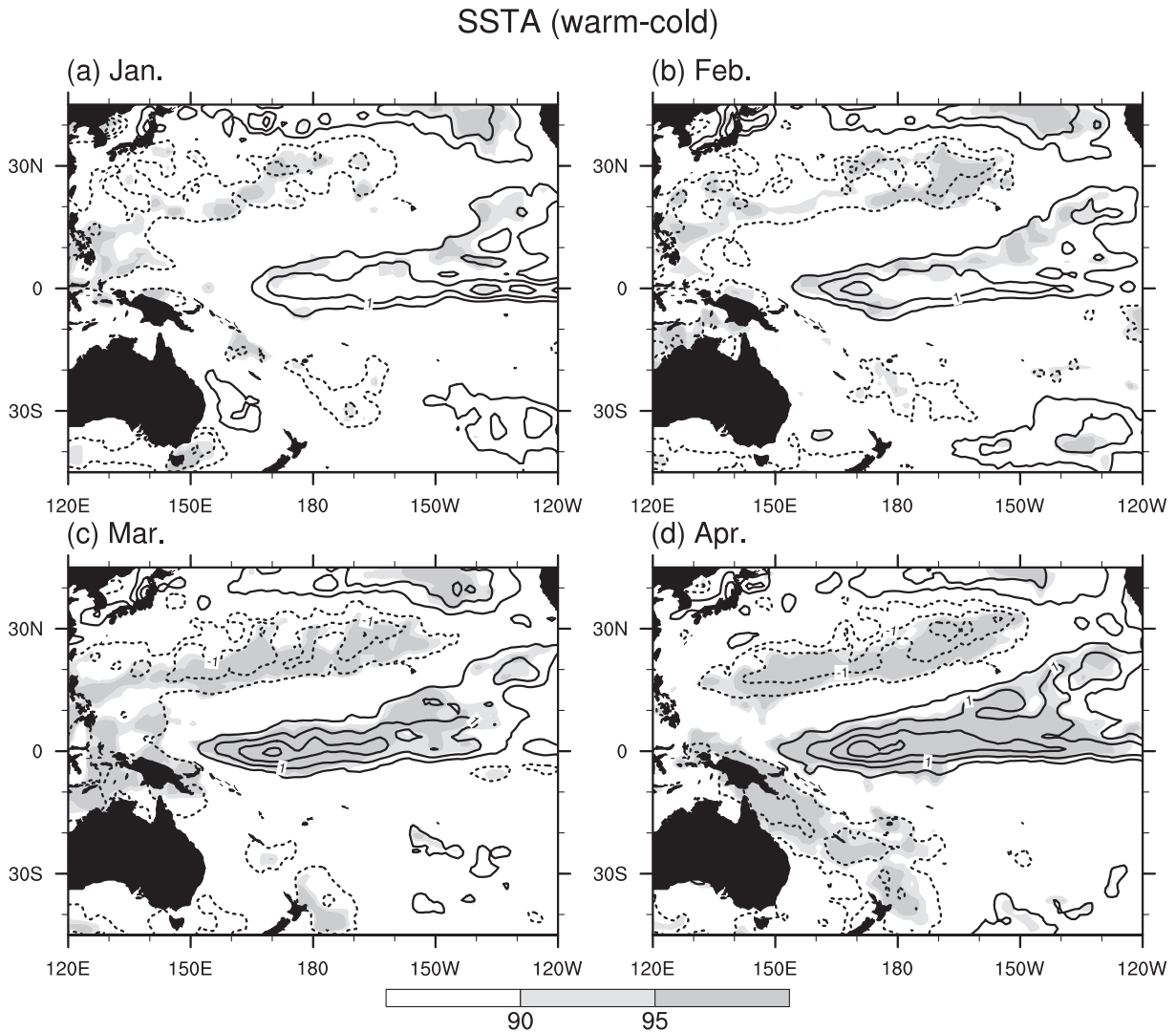


Fig. 2. Composite difference maps of SSTAs in (a) January, (b) February, (c) March, and (d) April between the five warm and three cold events of ENSO. The contour interval is 0.5 K. Zero contours are omitted. Anomalies exceeding the thresholds for significance at the 90% and 95% levels are indicated by light and dark shaded regions, respectively.

temporal evolutions of q'_a and q'^*_o tend to show similar behavior. Particularly from August to October, a decrease in q'_a follows a decrease in q'^*_o . Alexander et al. (2004) indicated that a reduced short wave radiation associated with an increase in low clouds is a major factor to form the negative SSTAs in the subtropical North Pacific during this period. Over the subtropical South Pacific, significant negative q'_a is formed in March and persists until November (Fig. 4b). Throughout this period, q'_a is lower than q'^*_o except for August, indicating that the anomalous

air–sea difference in specific humidity contributes to enhance evaporation from the ocean surface. During the same period, significant negative SSTAs less than -0.4°C actually persist over the subtropical South Pacific during the premature stage of the ENSO warm event (Figs. 4b, 1). These temporal evolutions of q'_a and q'^*_o suggest that the surface air humidity anomaly is important for the formation of negative SSTAs in the subtropical Pacific of both hemispheres.

In general, surface air humidity variation is

Surface air humidity and wind anomalies (warm-cold)

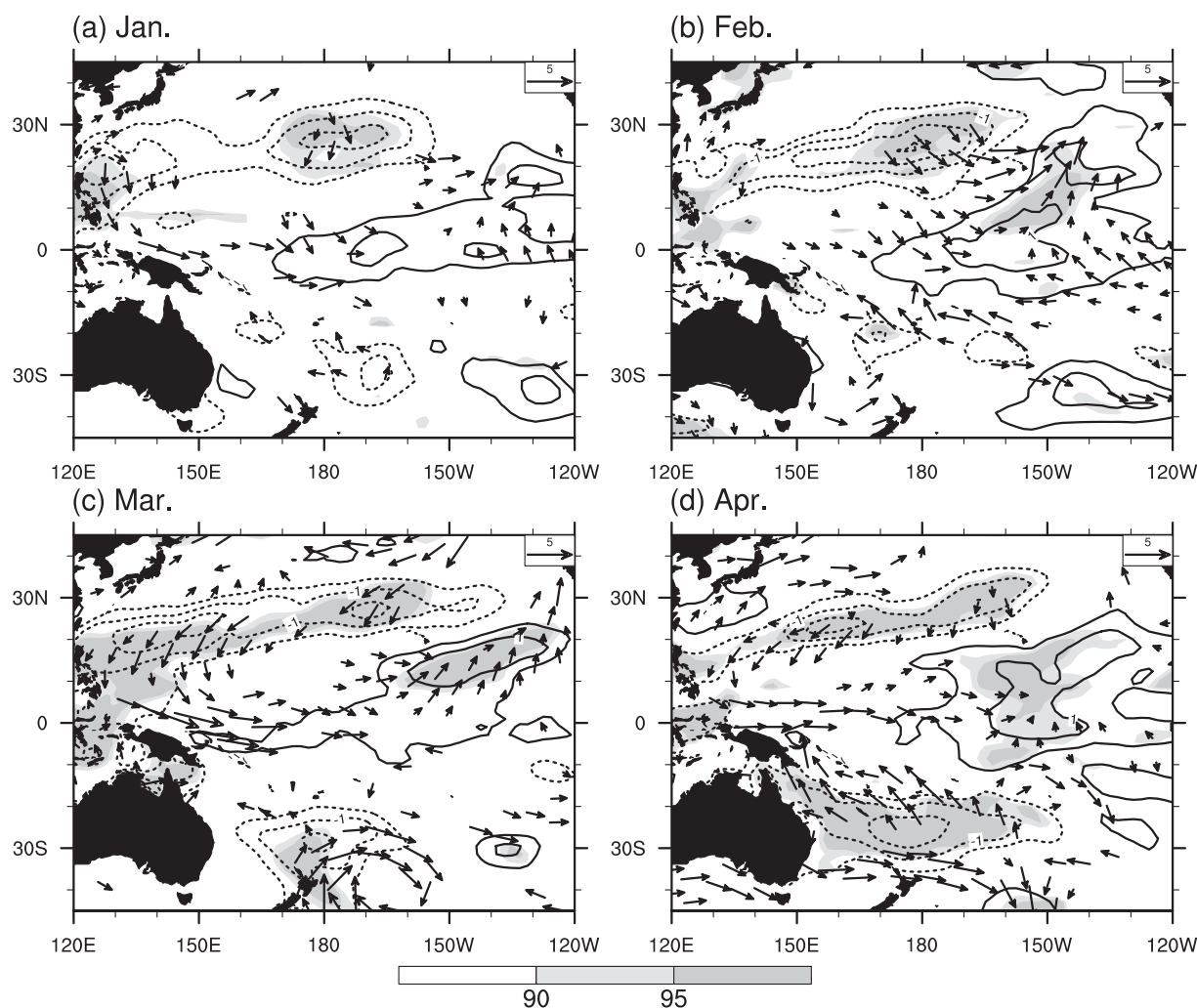


Fig. 3. Composite difference maps of air humidity anomalies at a 2-m height and surface wind anomalies in (a) January, (b) February, (c) March, and (d) April between the five warm and three cold events of ENSO. The contour interval is 0.5 g kg^{-1} and zero contours are omitted. The reference vector at the upper right corner indicates 5 m s^{-1} . Air humidity anomalies exceeding the thresholds for significance at the 90% and 95% levels are indicated by light and dark shaded regions, respectively. Wind vectors with either the zonal or meridional component exceeding the 90% significance level are plotted.

mainly controlled by local SSTAs over the tropics. Over the equatorial regions, for example, a positive SSTA leads to surface moist air associated with the development of ENSO (Figs. 2, 3). Over the subtropical regions, on the other hand, the negative SSTA follows the surface dry air, suggesting that surface air humidity variation associated with a change in atmospheric circulation induces the local SST variability. In fact, the equatorward surface

wind anomalies are observed over the subtropical negative air humidity anomalies at the same time. Therefore, we turn our attention to the relationship between surface air humidity anomaly and a change in the local Hadley circulation.

Figures 5a,b show the latitude–time diagrams of composite difference for surface humidity and vertical motion at 500 hPa zonally averaged over the 160°E – 170°W . The climatological cycle for these

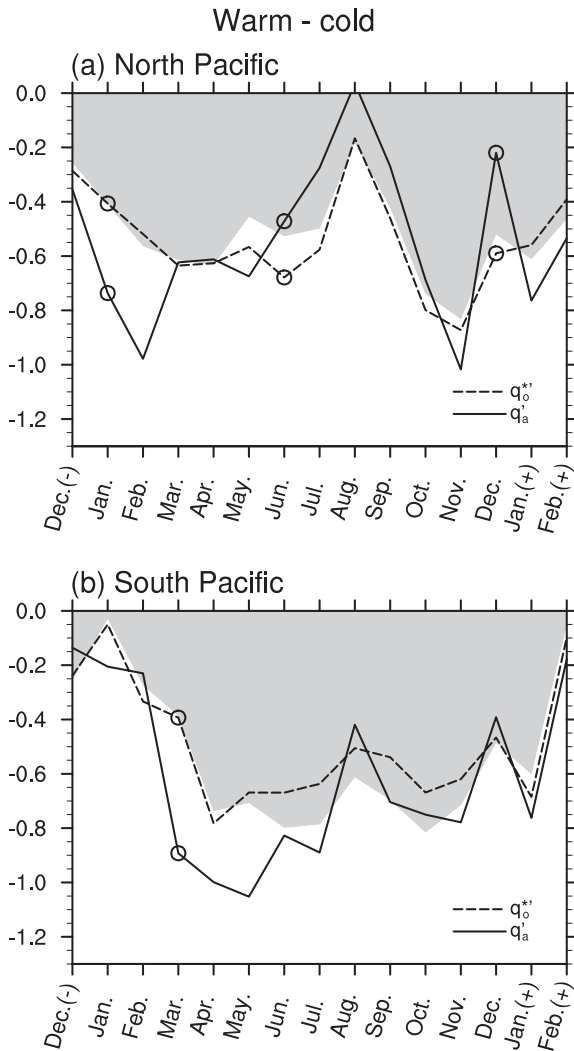


Fig. 4. Composite difference anomalies of air humidity at a 2-m height (q'_a ; solid line), saturation specific humidity at the sea surface (q^*_o ; dashed line), and SSTAs (shaded) averaged over (a) the subtropical North Pacific (20°N – 40°N , 160°E – 170°W) and (b) the subtropical South Pacific (20°S – 40°S , 160°E – 170°W) between the five warm and three cold events of ENSO. The units of specific humidity and SSTA are g kg^{-1} and K. Anomalies of the air-sea humidity difference exceeding the thresholds for significance at the 90% levels are indicated by circles.

variables is also shown in Figs. 5c,d. During the ENSO warm event, anomalous upward motion in the equator and downward motion in the subtropi-

cal North Pacific are observed in January and February (Fig. 5b), thereby strengthening the climatological local Hadley circulation in the Northern hemisphere (Fig. 5d). Associated with the strengthened climatological descending branch of local Hadley circulation, negative surface air humidity anomalies appear over the subtropical North Pacific during the dry season (Figs. 5a,c). In the following March and April, the anomalous downward motion begins to take place in the subtropical South Pacific associated with the seasonal cycle of the climatological descending branch, enforcing the local Hadley circulation in the Southern hemisphere. This anomalous downward motion over the subtropical South Pacific persists from March to September with the strengthened climatological local Hadley circulation in the Southern hemisphere, while the climatological local Hadley circulation in the Northern hemisphere disappears during this period. Associated with this transition of intensity in the climatological downward motion from the northern to the southern subtropics, a negative specific humidity anomaly (i.e., surface dry air) is prominent in the subtropical North Pacific during the January–February period and then appears in the subtropical South Pacific from March to September (Fig. 5a). Consistent with these transitions, the subtropical negative SSTAs are also formed in February in the subtropical North Pacific and in April in the subtropical South Pacific, respectively (Figs. 2, 4).

Figure 6 shows the latitude–vertical cross section of anomalous meridional circulation and specific humidity anomaly zonally averaged in 160°E – 170°W during the January–April period. As stated, air humidity anomalies are closely related to the anomalous meridional circulation: positive (negative) specific humidity anomaly with anomalous upward (downward) motion near the equator (subtropics). On the basis of these vertical cross sections, we also capture the seasonal transition of the anomalous meridional circulation. In the January–February period, the negative specific humidity anomaly and the anomalous downward motion are dominant in the Northern hemisphere around 25°N (Figs. 6a,b). These anomalies in the subtropical North Pacific accompany a positive humidity anomaly and an anomalous upward motion near the equator. In the following March, however, the amplitudes of these anomalies in the subtropical North Pacific gradually decrease (Fig. 6c). Instead, the anomalous downward motion and the negative

The western Pacific (160E-170W)

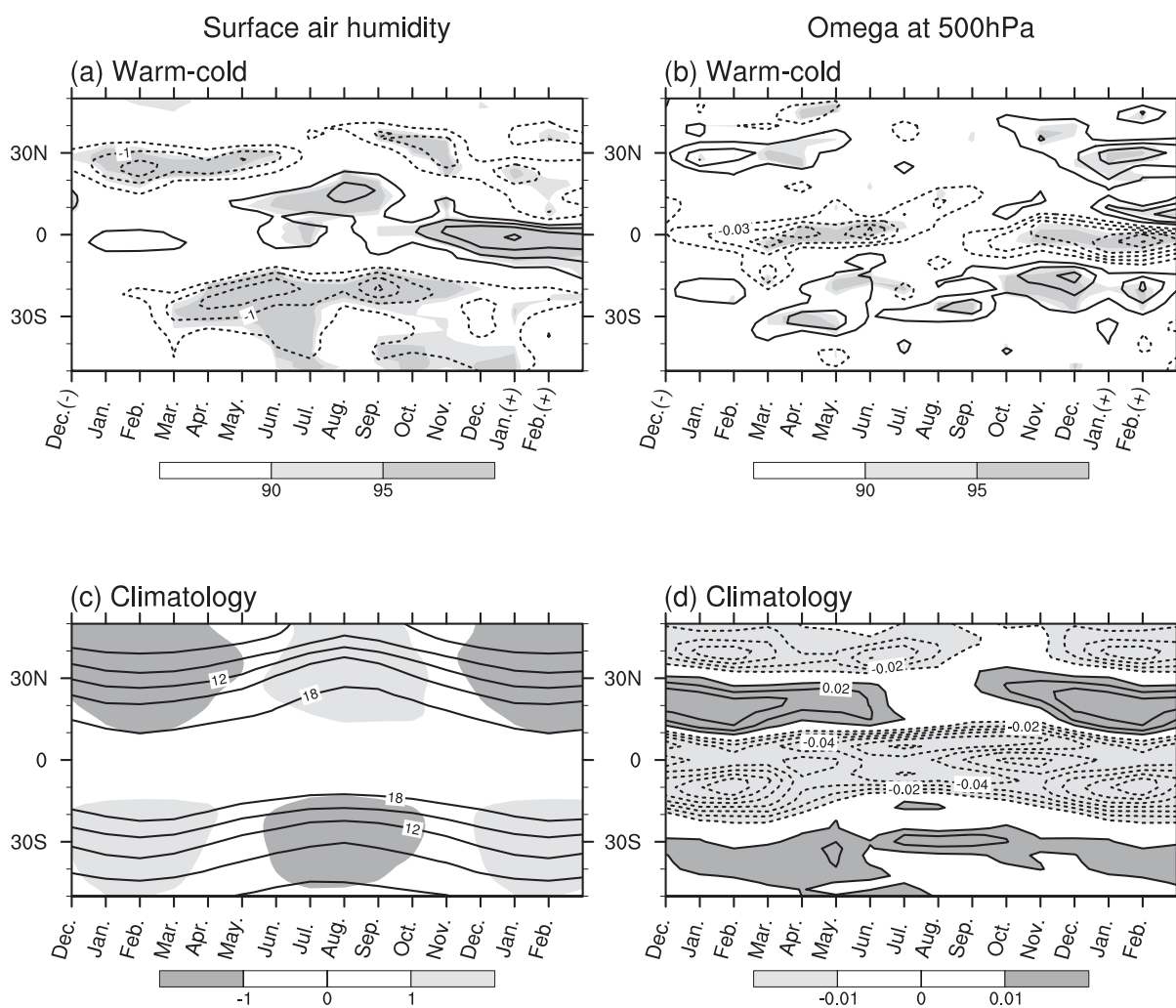


Fig. 5. Time evolution of air humidity at a 2-m height (left panels) and vertical p-velocity at 500 hPa (right panels) in (a,b) the composite difference between the five warm and three cold events of ENSO and (c,d) climatology. The deviations from annual means of climatological air humidity are shaded in (c). The units in the left and right panels are g kg^{-1} and Pa s^{-1} , respectively. Anomalies exceeding the thresholds for significance at the 90% and 95% levels are indicated by light and dark shaded regions, respectively.

specific humidity anomaly become prominent in the Southern hemisphere extending from 20°S to 40°S. This dry air in the lower atmosphere associated with the anomalous downward motion over the subtropical South Pacific amplifies and shifts equatorward in the following April (Fig. 6d).

During the premature stage of the ENSO events, equatorial positive SSTAs can induce the anomalous meridional circulation near the Date Line. This anomalous meridional circulation strengthens

the climatological local Hadley circulation and then causes the strengthened descending branch of local Hadley circulation. Associated with the seasonal cycle of climatological local Hadley circulation, the strengthened descending branch induced by the anomalous meridional circulation also shows the seasonal transition from the Northern to Southern hemisphere during the boreal spring. Since changes in the descending branch of the local Hadley circulation affect the surface air humidity

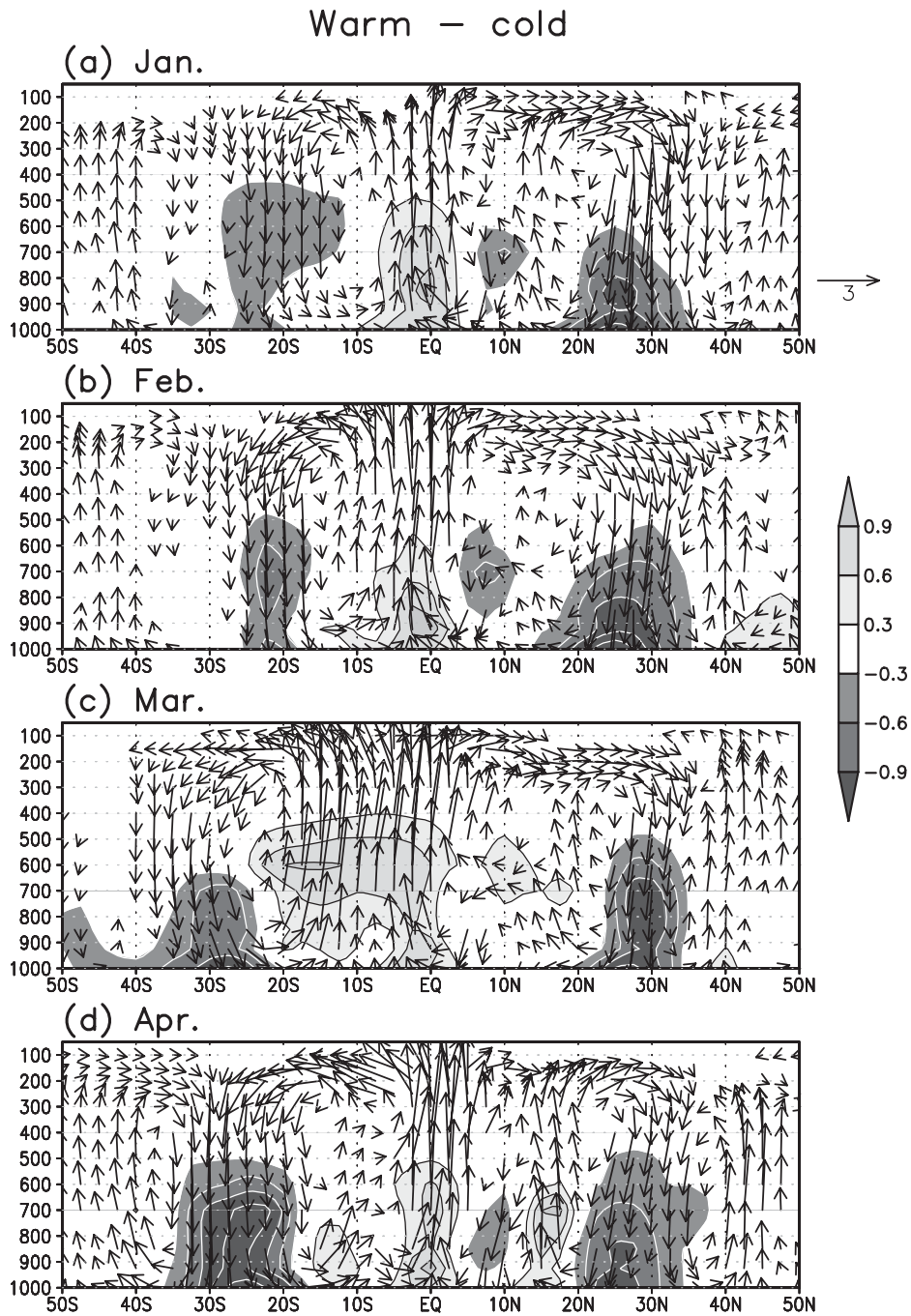


Fig. 6. Composite difference anomalies of meridional wind (m s^{-1}), vertical p-velocity (upward positive; $\times 10^{-2} \text{ Pa s}^{-1}$), and specific humidity (shaded) zonally averaged from 160°E to 170°W in (a) January, (b) February, (c) March, and (d) April between the five warm and three cold events of ENSO. The reference vector above the color bar is 3 m s^{-1} or $3 \times 10^{-2} \text{ Pa s}^{-1}$. The contour interval is 0.3 g kg^{-1} and zero contours are omitted.

variability, the observed negative air humidity anomalies in the subtropical Pacific also show the seasonal transition from the Northern to Southern hemisphere. As we stated in the introduction, the surface air humidity variability can induce the local SST variability through changes in surface evaporation. In the next section, we will examine the formation processes of the subtropical negative SSTAs induced by the surface air humidity anomalies.

4. Formation processes of the subtropical Pacific SSTAs

To examine the formation process of negative SSTA in the subtropical North Pacific, we draw composite maps of SSTA tendency and net heat flux anomaly in January (Fig. 7). The SSTA tendency in a given month is defined as the difference between the SSTA in the subsequent month and that in the previous month. A positive heat flux anomaly indicates a heat loss from the ocean surface. Since the surface latent and sensible heat fluxes in the reanalysis data are less reliable than other elements in the free atmosphere, we will also examine the COADS dataset. In both datasets, decreases in SSTA of 0.3°C for two months are observed in the subtropical North Pacific with a zonally elongated pattern along 25°N (Figs. 7a,b). Over this region, positive net heat flux anomalies of 20 W m^{-2} are also observed in both datasets (Figs. 7c,d), although those anomalies are somewhat stronger in NCEP2. Given that SSTA tendencies of -0.3°C for 2-month are only due to surface heat flux anomalies of 20 W m^{-2} , we obtain an equivalent mixed layer depth of 85-m, comparable to the observed isothermal layer in the subtropical North Pacific in January (Kara et al. 2003). This estimation suggests that the January surface heat flux anomaly mainly contributes to the formation of the negative SSTA in this region.

Over the tropics, a primarily important component of net heat flux anomaly is a latent heat flux anomaly, particularly induced by a change in wind speed (e.g., Cayan 1992; Alexander and Scott 1997; Xie et al. 1999). Indeed, the January composite map of heat flux anomaly component indicates that positive latent heat flux anomalies of 20 W m^{-2} are observed over the subtropical North Pacific with the zonally elongated pattern along 25°N while short wave radiation anomaly is quite small over most of the North Pacific during this period (Fig. 7e-h). However, as stated below, the anomalous scalar wind speed is insufficient in ex-

plaining the latent heat flux anomalies over the subtropical North Pacific.

The latent heat flux anomaly can be decomposed into three linearized components as in Enfield and Mayer (1997) and Tanimoto et al. (2003):

$$F'_{lh} = \rho c_e L_e \{ W' \overline{\Delta q} + \overline{W} \Delta q' + (W' \Delta q' - \overline{W' \Delta q'}) \}, \quad (1)$$

where F_{lh} is the latent heat flux, W is the scalar wind speed, Δq is the air-sea difference in specific humidity, ρ is the atmospheric density, c_e is the bulk coefficient, L_e is the latent heat of vaporization for water, and the overbar and prime indicate the climatological mean and anomaly, respectively. The bulk coefficients are assumed to be constant in NCEP2 and to be dependent on scalar wind speed and static stability in COADS. However, when we linearize the surface heat flux anomalies, we ignore the dependence of the coefficients on those variables. On the right-hand side of (1), the first two terms represent contributions of the wind speed anomaly (W' component) and the anomalous air-sea difference in specific humidity ($\Delta q'$ component) to the total amount of latent heat flux anomalies, respectively. The sum of these first two terms (Figs. 8e,f) is comparable to the total latent heat flux anomaly (Figs. 7e,f) and explains most of the net heat flux anomalies (Figs. 7c,d).

Figure 8 shows the January composite maps of the linearized components of latent heat flux anomalies based on COADS and NCEP2-OISST datasets. In both datasets, positive anomalies of W' component are observed with the zonally elongated pattern along 25°N (Figs. 8a,b). Positive anomalies of $\Delta q'$ component are also observed over the subtropical North Pacific particularly near the Date Line (Figs. 8c,d). As a result, the latent heat flux anomalies with the zonally elongated pattern along 25°N , approximately represented by sum of these two components, enhance the heat loss from the subtropical North Pacific Ocean and then contribute to the formation of negative SSTAs. These results indicate that the $\Delta q'$ and W' components, is important for generating a substantial latent heat flux anomaly in January, and hence, negative SSTAs in the following February over the subtropical North Pacific.

To examine the formation of the negative SSTAs in the subtropical South Pacific from February to April, we drew composite maps of SSTA tendency and net heat flux anomaly in March (Fig. 9). In

The North Pacific (Jan.)

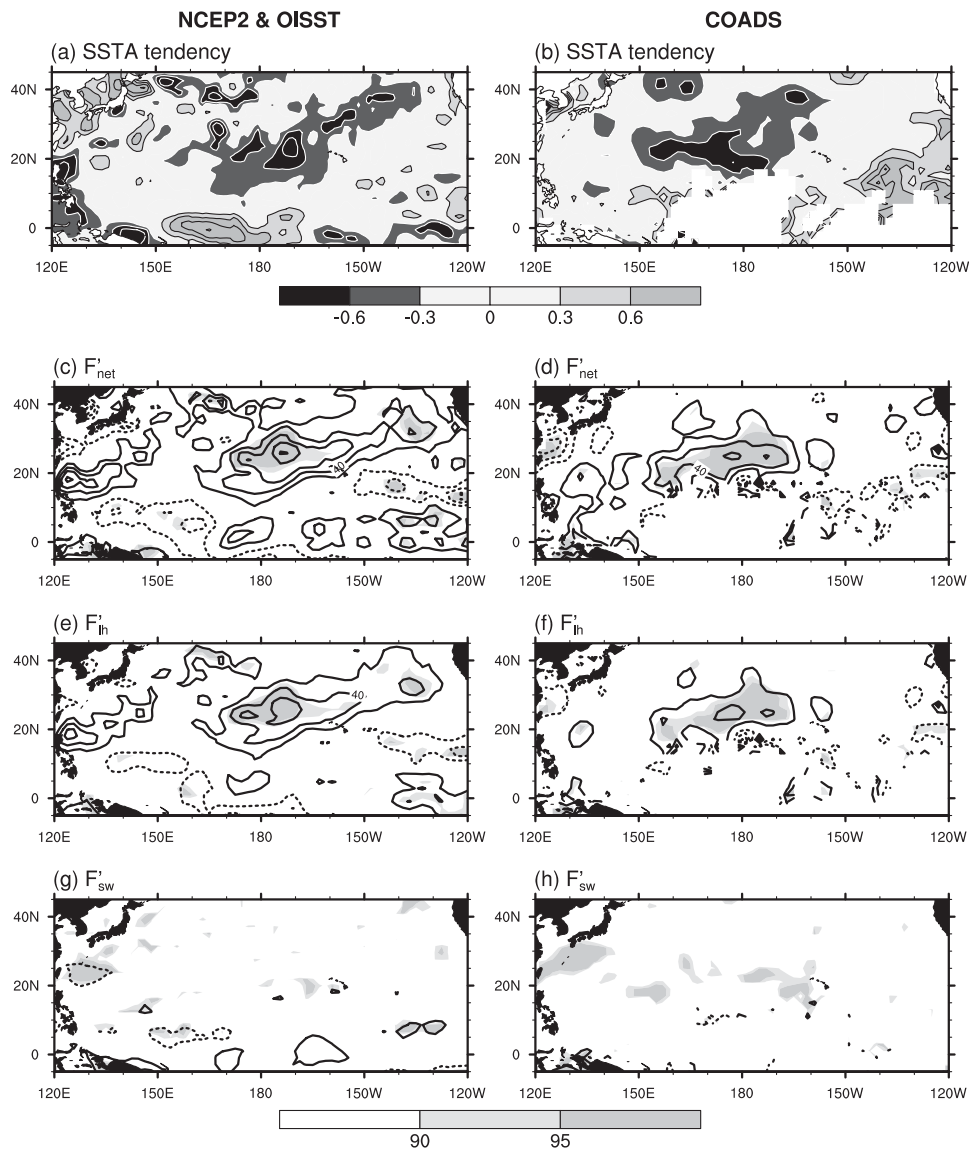


Fig. 7. Composite difference maps of (a,b) SSTA tendency, (c,d) surface net heat flux anomaly, (e,f) latent heat flux anomaly, and (g,h) short wave radiation anomaly in January between the ENSO warm and cold events. The left (right) panels are based on NCEP2 and OISST (COADS) in five (seven) warm and three (seven) cold events of ENSO. The SSTA tendency in a given month is defined as the difference between the SSTA in the subsequent month and that in the previous one. Positive anomalies in surface heat flux indicate heat loss from the ocean. The contour intervals of SSTA tendency (heat flux anomalies) are 0.3 K ($20 W m^{-2}$) and zero contours are omitted. Heat flux anomalies exceeding the thresholds for significance at the 90% and 95% levels are indicated by light and dark shaded regions, respectively.

both datasets, decreases in SSTA of $0.6^{\circ}C$ for two months are observed in the South Pacific extending from the equator to $40^{\circ}S$ and tilting southeastward (Figs. 9a,b). Over this region, positive net heat flux

anomalies of $40 W m^{-2}$ are also observed in both datasets (Figs. 9c,d). The observed isothermal layer over this region is at about a 50-m, depth almost comparable to the equivalent mixed layer depth

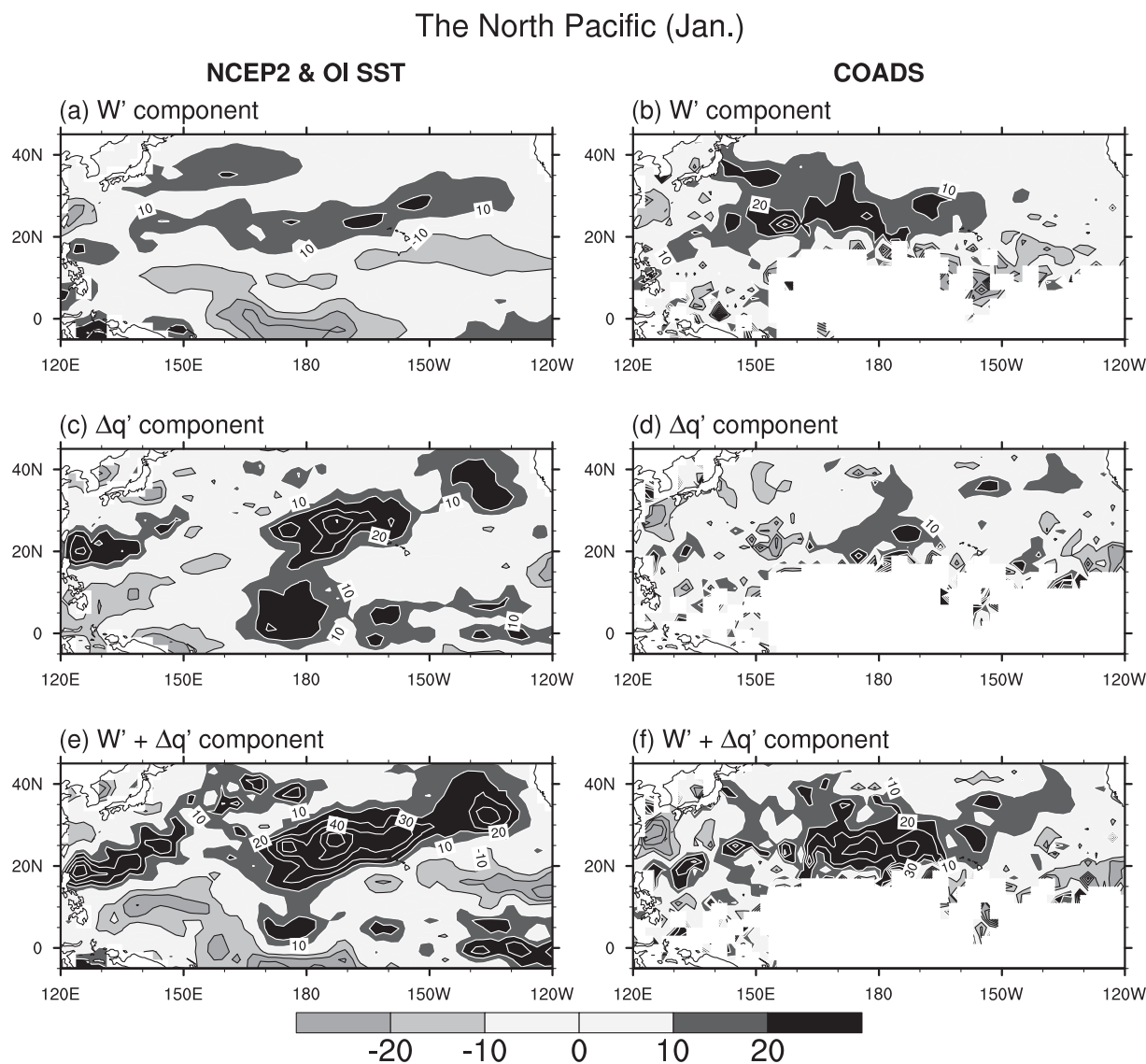


Fig. 8. Composite difference maps of contributions of (a,b) wind speed anomaly and (c,d) anomalous air-sea difference in specific humidity to latent heat flux anomaly and (e,f) sum of these two contributions in January. The left (right) panels are based on NCEP2 and OI SST (COADS) in five (seven) warm and three (seven) cold events of ENSO. The contour interval is 10 W m^{-2} , which is half for Fig. 7. Zero contours are omitted.

obtained from those anomalies. Over the tropical Pacific, a significant westerly wind anomaly appears along 10°S over the western tropical Pacific in March (Fig. 3c). These westerly wind anomalies can enhance the surface wind speed, and therefore contribute to the positive latent heat flux anomaly. To the east of Australia, on the other hand, the surface wind anomaly is weak in March (Fig. 3c), while significant negative SSTAs are observed in

the following April (Fig. 2d). This result suggests the relative importance of $\Delta q'$ for generating negative SSTAs in the subtropical South Pacific, similar to the subtropical North Pacific.

Figure 10 shows March composite maps of the linearized components of latent heat flux anomalies. The net heat flux anomaly that is mainly contributed by the latent heat flux anomaly is well represented by the sum of the W' and $\Delta q'$ components

The South Pacific (Mar.)

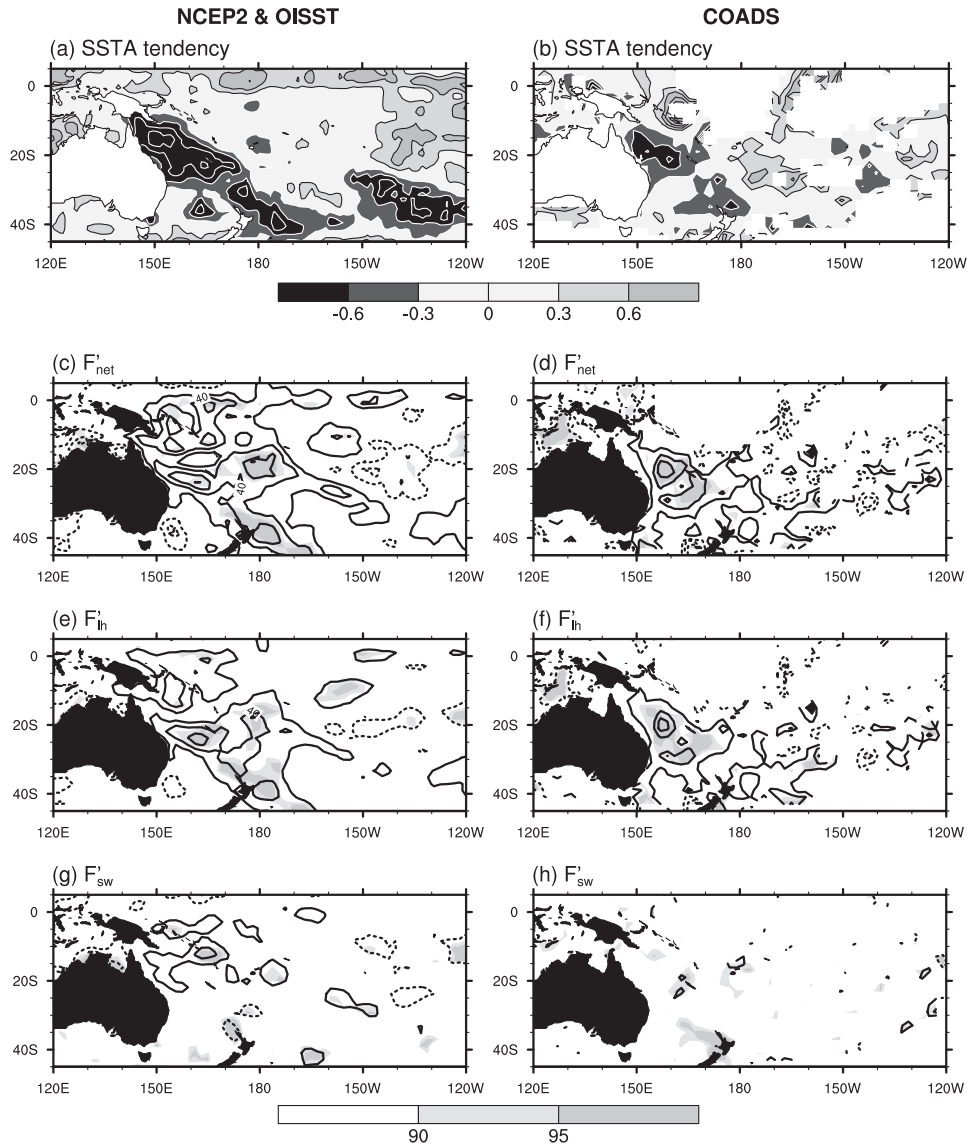


Fig. 9. Figure legends are the same as those in Fig. 7, but for March.

(Figs. 9, 10e,f). In NCEP2 and OISST, the positive latent heat flux anomaly over the South Pacific is mainly contributed by the W' component north of 20°S, but by the $\Delta q'$ component south of 20°S (Figs. 10a,c). As a result the positive latent heat flux anomalies have a meridionally large area extending equator to 40°S. In COADS, the positive anomalies of the $\Delta q'$ component south of 20°S are also observed, while there are many missing values

north of 20°S (Figs. 10b,d). These results indicate that the $\Delta q'$ component is important for generating a substantial latent heat flux anomaly in March and hence negative SSTAs in the following April over the subtropical South Pacific.

Over the tropics, SSTAs are normally higher than surface air temperature anomalies, implying that surface anomalies in humidity and temperature are caused by SSTAs. Over the equatorial Pacific,

The South Pacific (Mar.)

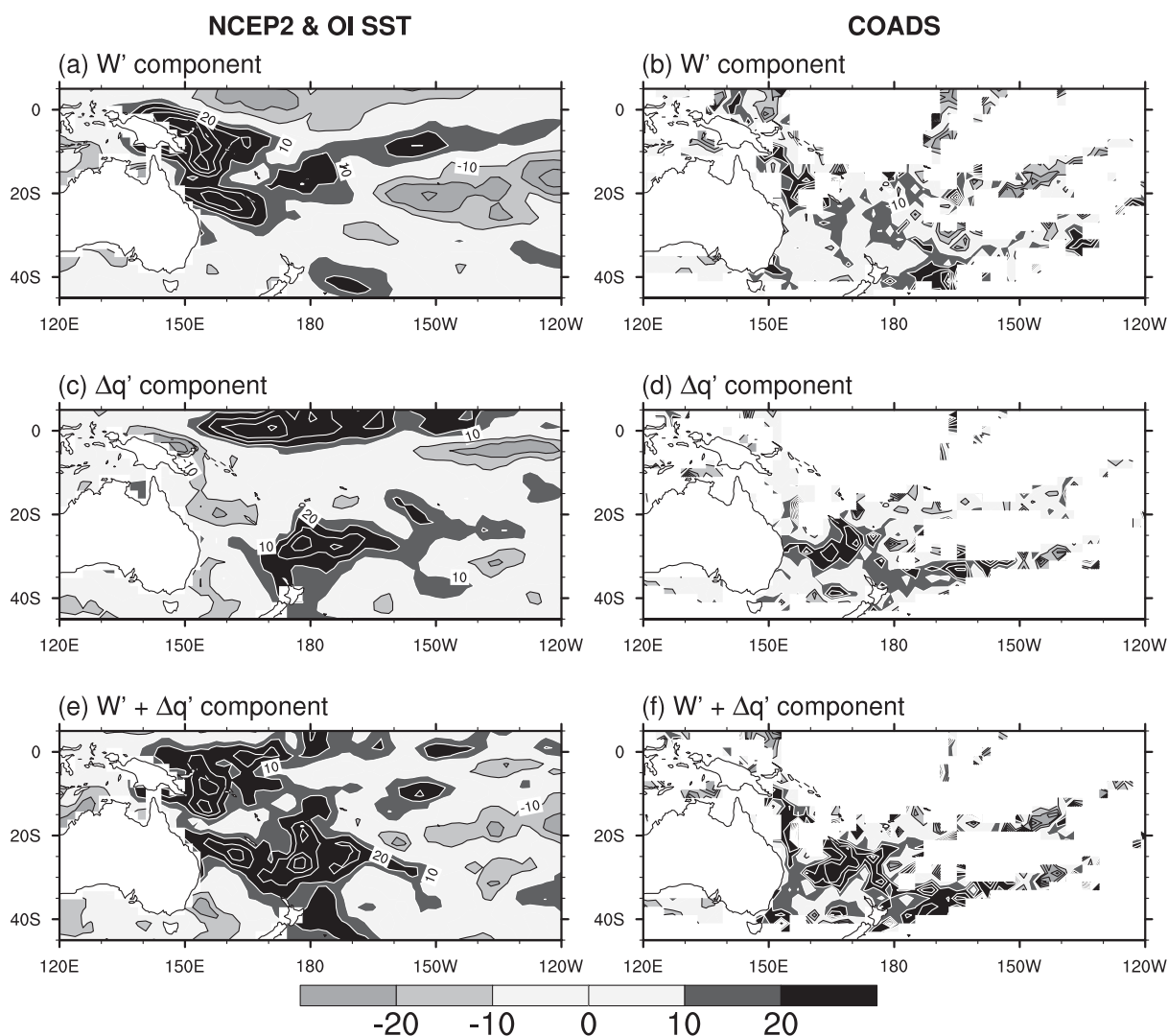


Fig. 10. Figure legends are the same as these in Fig. 8, but for March.

for example, SSTAs and $\Delta q'$ component show the same polarity (Figs. 2c, 10c), indicating that a positive SSTa induces positive air humidity due to enhanced surface evaporation. Over the subtropics, however, SSTAs and $\Delta q'$ component show opposite polarities in the subtropical North Pacific in January (Figs. 2a, 8c) and in the subtropical South Pacific in March (Figs. 2c, 10c). These results indicate that a negative air humidity anomaly can produce the positive anomaly of $\Delta q'$ component, and therefore induce negative SSTAs in the subtropics.

5. Discussion

To understand the subtropical air-sea interaction, we will discuss the role of the anomalous downward motion related to the strengthened local Hadley circulation. The anomalous downward motion can induce a dry condition in the lower atmosphere due to moisture flux advection, which affects the formation of subtropical negative SSTAs through the contribution from anomalous air-sea humidity difference to latent heat flux anomaly,

as stated in the previous section. In fact, q'_a is significantly anti-correlated with vertical p-velocity at 500 hPa in January and February over the subtropical North Pacific (correlation coefficients r are -0.65 and -0.59 , respectively, and exceed the statistical significance at the 99% level) and in March and April over the subtropical South Pacific ($r = -0.56$ and -0.76). The anomalous downward motion associated with the strengthened local Hadley circulation coincides with the local maxima of equatorward surface wind anomalies in January over the subtropical North Pacific and in March over the subtropical South Pacific, which locates in a slightly poleward region of the low-level return flow of the local Hadley circulation (Figs. 3, 6). This relationship between the anomalous downward motion and the equatorward surface wind anomaly satisfies the Sverdrup balance. Therefore, these vertical and meridional wind anomalies in the subtropics can effectively induce a dry condition in the lower atmosphere due to vertical and horizontal moisture flux advection, and cause enhanced evaporation from the ocean surface in these regions.

The enhanced evaporation induced by the anomalous downward motion also affects the moisture balance. The moisture budget equation shows a balance among a vertically integrated moisture flux divergence, evaporation from the ocean surface, and precipitation as follow:

$$\int_0^{P_s} \nabla \cdot (q\mathbf{V})' = E' - P'. \quad (2)$$

Under the descending branch of the local Hadley circulation, however, the precipitation variation is small when compared to the other terms. Therefore, the enhanced evaporation mainly balances the vertically integrated moisture flux anomaly divergence over the subtropical region associated with the anomalous downward motion. Table 1 shows each term of the moisture budget equation averaged over regions (20°N – 40°N , 160°E – 170°W) of the subtropical North Pacific in January and (40°S – 20°S , 160°E – 170°W) of the subtropical South Pacific in March. Note that the left-hand side of Eq. (2) is estimated by the vertical integration of the moisture flux anomaly divergence from the surface to 700-hPa. As we have suggested, the magnitude of the evaporation anomaly is almost comparable to that of moisture flux anomaly divergence in the lower atmosphere over these regions, while the precipitation anomaly is much smaller

than those terms. Since the moisture flux anomaly divergence in the lower atmosphere is closely related to the anomalous downward motion, the anomalous downward motion in the subtropics can affect the enhanced evaporation from the ocean surface through the anomalous wind divergence in the lower atmosphere.

On the basis of these balances, the role of air-sea interaction in the subtropical Pacific is explained as follows. During the premature stage of the ENSO warm event, the growth of equatorial SSTAs will drive an anomalous downward motion in the subtropics associated with the strengthened local Hadley circulation. This anomalous downward motion accompanies an equatorward wind anomaly in the lower atmosphere at the same location to satisfy the Sverdrup balance. These anomalous downward motion and equatorward wind anomaly induce a dry condition in the lower atmosphere due to vertical and horizontal moisture advections, which in turn cause enhanced evaporation from the ocean surface. During the dry season in the subtropical Pacific, the enhanced evaporation balances the vertically integrated moisture flux divergence mainly contributed from the wind anomaly divergence in the lower atmosphere, implying a low-level return flow of the local Hadley circulation would be strengthened in the off-equatorial regions. In other words, the subtropical moisture associated with the enhanced evaporation from the ocean surface is transported to the equator by the low-level equatorward wind anomaly in the off-equatorial regions. Actually, the meridional component of the moisture flux anomaly in the lower atmosphere shows the equatorward moisture transports around 20° after the enhanced evaporation in the subtropics (Fig. 11). If this equatorward moisture transport can contribute to a strengthened initial local Hadley circulation due to the increasing moisture supply in the equatorial lower atmosphere, the process described above indicates the presence of an atmospheric positive feedback loop. However, it is still unclear whether this positive feedback plays a significant role in the activity of Hadley circulation and/or has a ENSO phase dependency. To reveal the dynamical processes and causality involved in the subtropical air-sea interaction, further data diagnosis and model experimentation is required.

This atmospheric positive feedback would be suppressed by the subtropical negative SSTAs associated with an atmosphere-ocean interaction. Once the atmospheric positive feedback becomes active,

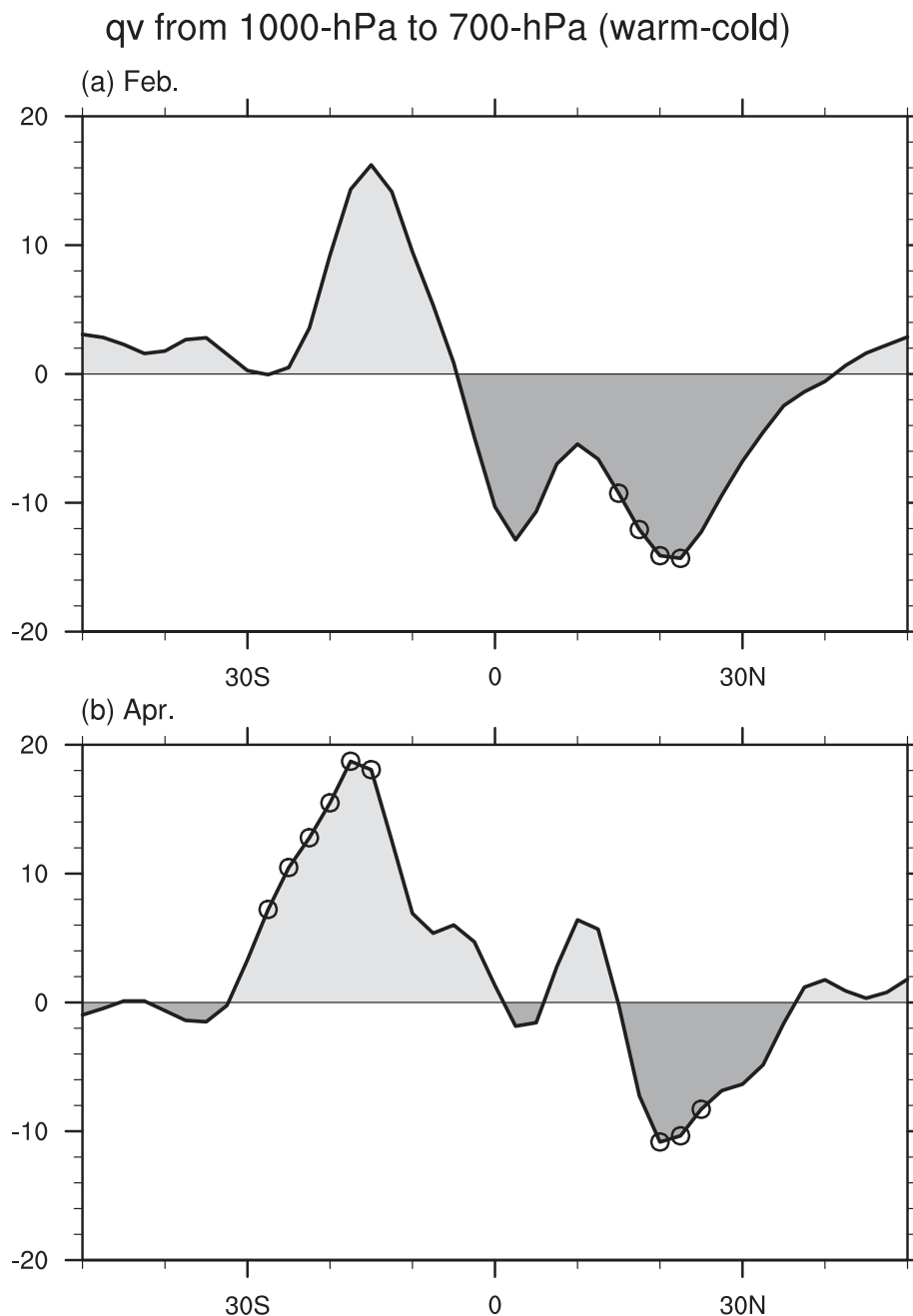


Fig. 11. Composite difference anomalies of the meridional component of vertically integrated moisture flux from the surface to 700-hPa (zonally averaged from 160°E to 170°W) in (a) February and (b) April between the five warm and three cold events of ENSO. Anomalies exceeding the thresholds for significance at the 90% levels are indicated by circles. Anomalies are normalized by atmospheric thickness, and their unit is $\text{g kg}^{-1} \text{m s}^{-1}$. Northward (southward) anomalous moisture transport is light (dark) shaded.

the enhanced evaporation accompanied by this feedback induces negative SSTAs in the subsequent month. Since the negative SSTAs reduce the ampli-

tude of enhanced evaporation through the reduction of air-sea humidity difference, the atmospheric positive feedback would not be strengthened due

to this SSTA damping effect. According to this process, SSTAs act to adjust to the surface air humidity anomaly associated with the atmospheric positive feedback. This idea is similar to the regulatory mechanism suggested by Chiang and Lintner (2005), who examined the gross oceanic and land surface temperature warming in the entire tropics after the mature stage of the ENSO warm event. If the strengthened descending branch of the local Hadley circulation retains the subtropical enhanced evaporation, the subtropical negative SSTAs may be maintained during the premature stage of the ENSO warm event. During the subtropical wet season, however, the atmospheric feedback becomes inactive because of the large precipitation amount that induces a new moisture balance. This could be a reason why negative SSTAs in the subtropical regions show seasonal variations associated with the local Hadley circulation.

6. Summary

We have examined the formation processes of negative (positive) SSTAs in the subtropical North and South Pacific during the premature stage of the ENSO warm (cold) events from reanalysis and in-situ observational datasets. Our composite difference maps between the ENSO warm and cold events indicate that significant negative SSTAs are observed over the subtropical North Pacific near the Date Line in February–March period and over the subtropical South Pacific after April. One month before the formation of these subtropical negative SSTAs, negative air humidity anomalies appear at the same location of these subtropical negative SSTAs in both hemispheres. Our analysis shows that the subtropical negative air humidity anomalies accompany the anomalous downward motion that corresponds to the strengthened descending branch of the local Hadley circulation. These negative air humidity anomalies and anomalous downward motion show a seasonal transition from the Northern hemisphere in the January–February period to the Southern hemisphere in the March–April period. This transition in anomalous surface dry air and downward motion from the Northern to Southern hemisphere has the same timing to climatological seasonal cycle for the descending branch of the local Hadley circulation. These results suggest that the negative air humidity anomalies associated with the strengthened descending branch of the local Hadley circulation can induce negative SSTAs in the subtropics

through an enhanced latent heat flux at the sea surface. Our linear decomposition analysis of surface heat flux anomalies indicate that the enhanced latent heat flux contributed by anomalous air-sea humidity difference, as much as by anomalous scalar wind speed, is the major factor to form the subtropical negative SSTAs in both hemispheres.

Over the tropical ocean such as the climatologically warm SST region an anomalous vertical motion is mainly controlled by local SSTAs. In the equatorial Pacific, for example, SSTAs and anomalous air-sea humidity difference show the same polarity (Figs. 2c, 10c), implying that the equatorial SST variability affects the intensity in the equatorial upward motion because of atmospheric dynamic and thermodynamic responses. Over the subtropics, however, anomalous downward motion plays an important role in the formation of subtropical SSTAs through surface air humidity anomalies. According to the principle of Sverdrup balance, an anomalous downward motion in the middle troposphere accompanies the equatorward surface wind anomaly in the subtropics. These anomalous downward motion and equatorward surface wind anomaly contribute to induce the dry condition in the lower atmosphere through vertical and horizontal moisture flux advectations and then cause the negative SSTAs through the enhanced evaporation at the sea surface. As expected from these processes in the lower atmosphere, SSTAs and anomalous air-sea humidity difference show an opposite polarity in the subtropical North Pacific in January (Figs. 2a, 8c) and in the subtropical South Pacific in March (Figs. 2c, 10c). On the basis of the moisture budget equation, the anomalous moisture flux divergence related to the anomalous downward motion mostly balances the enhanced

Table 1. Each term of the moisture budget equation averaged in the subtropical North Pacific (NP; 20°N–40°N, 160°E–170°W) and South Pacific (SP; 20°S–40°S, 160°E–170°W). The moisture flux anomaly divergence is estimated by the vertical integration of moisture flux anomaly divergence from surface to 700-hPa. Anomalies of vertically integrated moisture flux divergence, evaporation, and precipitation represent $\nabla \cdot (q\mathbf{V})'$, E' , and P' in units of mm day^{-1} , respectively.

	Month	$\nabla \cdot (q\mathbf{V})'$	E'	P'
NP	Jan	1.28	0.91	−0.35
SP	Mar	1.22	1.09	−0.13

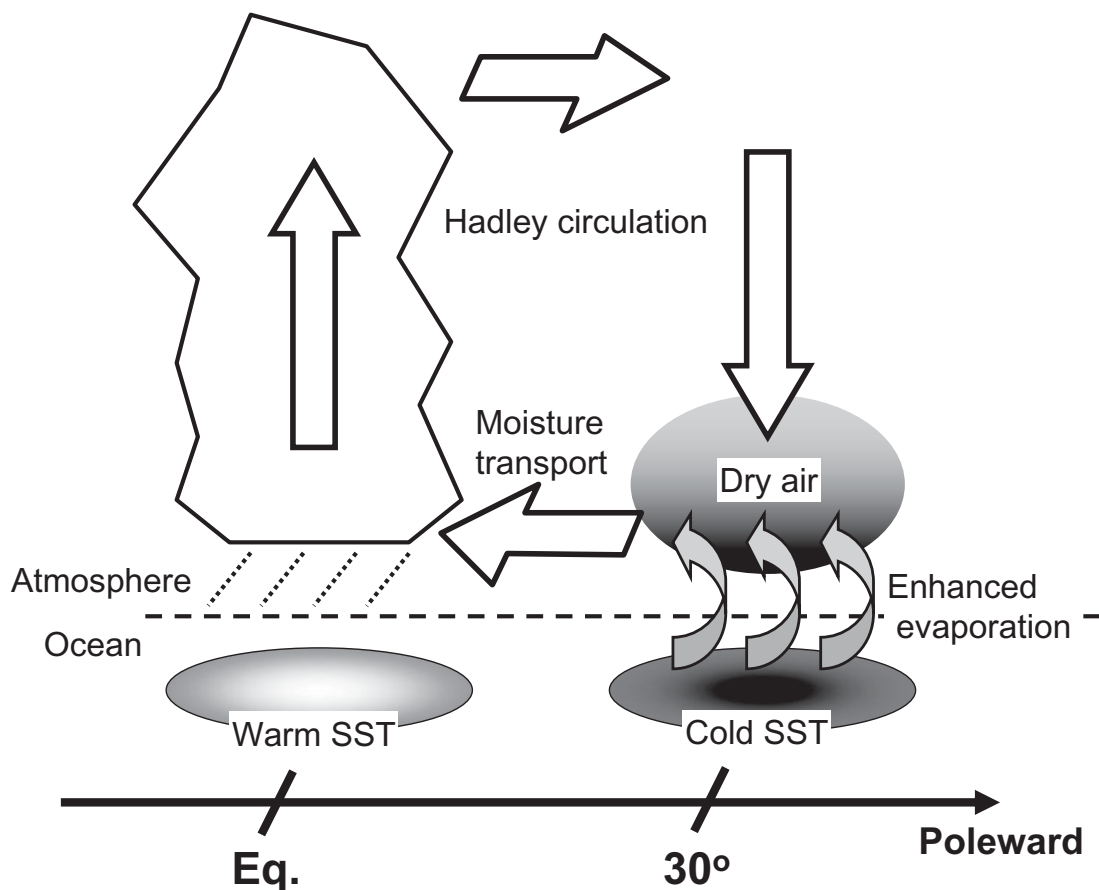


Fig. 12. Schematic diagram of the proposed atmosphere-ocean interaction near the Date Line during the premature stage of the ENSO warm event. The white open arrows indicate the strengthened vertical and meridional winds associated with the local Hadley circulation.

evaporation at the sea surface because the precipitation anomaly is small under the climatological descending branch of the local Hadley circulation (Table 1). This relationship between anomalous downward motion and SSTA will be the unique characteristic of subtropical air-sea interaction when compared to the tropics. On the basis of the results of our analysis, we discussed a possible feedback loop in the subtropical atmosphere, which is summarized in the schematic diagram in Fig. 12. This atmospheric positive feedback could be a reason why the negative SSTAs in the subtropical South Pacific persist for the half year during the premature stage of the ENSO events.

As we have seen in Section 4, the short wave radiation anomaly plays a minor role in the formation of subtropical SSTA in the NCEP2 and COADS datasets (Figs. 7, 9). However, Alexander et al. (2004) claimed that the short wave radiation

obtained from the reanalysis dataset has large errors. In addition, the number of surface observations in the South Pacific is not very large in the COADS dataset. Accurate surface observations of surface heat flux components are highly desired to reveal the mechanism underlying subtropical air-sea interaction.

Acknowledgments

The authors are grateful to S.-P. Xie, and M. Watanabe for their stimulating discussions. The manuscript benefitted from the constructive comments by anonymous reviewers. The NCEP2 and NOAA OI SST datasets were obtained from the website of the NOAA/OAR/ESRL PSD, Boulder, Colorado, USA, (<http://www.cdc.noaa.gov/>). This work was supported by Kakushin project of the Japanese ministry of education, culture, sports, science, and technology.

References

- Alexander, M. A., N.-C. Lau, and J. D. Scott, 2004: Broadening the atmospheric bridge paradigm, ENSO teleconnections to the tropical west Pacific-Indian Oceans over the seasonal cycle and to the North Pacific in summer. *Earth Climate: Ocean-atmosphere interaction and climate variability*, **147**, geophysical Monograph, AGU, Washington D. C., 85–103.
- Alexander, M. A., and J. D. Scott, 1997: Surface flux variability over the North Pacific and North Atlantic oceans. *J. Climate*, **10**, 2963–2978.
- Cayan, D. R., 1992: Latent and sensible heat flux anomalies over the northern oceans, The connection to monthly atmospheric circulation. *J. Climate*, **5**, 354–369.
- Chiang, J. C. H., and B. R. Lintner, 2005: Mechanisms of remote tropical surface warming during El Niño. *J. Climate*, **18**, 4130–4149.
- Chikamoto, Y., and Y. Tanimoto, 2005: Role of specific humidity anomalies in Caribbean SST response to ENSO. *J. Meteor. Soc. Japan*, **83**, 959–975.
- Chikamoto, Y., and Y. Tanimoto, 2006: Air-sea humidity effects on the generation of tropical Atlantic SST anomalies during the ENSO events. *Geophys. Res. Lett.*, **33**, L19 702, doi:10.1029/2006GL027238.
- Enfield, D. B., and D. A. Mayer, 1997: Tropical Atlantic sea surface temperature variability and its relation to El Niño-Southern Oscillation. *J. Geophys. Res.*, **102**, 929–945.
- Gu, D.-F., and S. G. H. Philander, 1997: Interdecadal climate fluctuations that depend on exchanges between the Tropics and extratropics. *Science*, **275**, 805–807.
- Kanamitsu, M., W. Ebisuzaki, J. Woollen, S.-K. Yang, J. J. Hnilo, M. Fiorino, and G. L. Potter, 2002: NCEP-DOE AMIP-II reanalysis (R-2). *Bull. Amer. Meteor. Soc.*, **83**, 1631–1643.
- Kara, A. B., P. A. Rochford, and H. E. Hurlburt, 2003: Mixed layer depth variability over the global ocean. *J. Geophys. Res.*, **108**, doi:10.1029/2000JC000736.
- Kawamura, R., Y. Fukuta, H. Ueda, T. Matsuura, and S. Iizuka, 2002: A mechanism of the onset of the Australian summer monsoon. *J. Geophys. Res.*, **107**, 4204.
- Kug, J. -S., and I. -S. Kang, 2006: Interactive feedback between the Indian Ocean and ENSO. *J. Climate*, **19**, 1784–1801.
- Larkin, N. K., and D. E. Harrison, 2002: ENSO warm (El Niño) and cold (La Niña) event life cycles: Ocean surface anomaly patterns, their symmetries, asymmetries, and implications. *J. Climate*, **15**, 1118–1140.
- Liu, Z., S. G. H. Philander, and P. C. Pacanowski, 1994: A GCM study of tropical-subtropical upper-ocean water exchange. *J. Phys. Oceanogr.*, **24**, 2606–2623.
- McCreary, J. P. J., and P. Lu, 1994: Interaction between the subtropical and equatorial ocean circulations: The subtropical cell. *J. Phys. Oceanogr.*, **24**, 466–497.
- Ohba, M., and H. Ueda, 2007: An impact of SST anomalies in the Indian Ocean in acceleration of the El Niño to La Niña transition. *J. Meteor. Soc. Japan*, **85**, 335–348.
- Oort, A. H., and J. J. Yienge, 1996: Observed interannual variability in the Hadley circulation and its connection to ENSO. *J. Climate*, **9**, 2751–2767.
- Rasmusson, E. M., and T. H. Carpenter, 1982: Variations in tropical sea surface temperature and surface wind fields associated with the Southern Oscillation/El Niño. *Mon. Wea. Rev.*, **110**, 354–384.
- Reynolds, R. W., N. A. Rayner, T. M. Smith, D. C. Stokes, and W. Wang, 2002: An improved in situ and satellite SST analysis for climate. *J. Climate*, **15**, 1609–1625.
- Shin, S.-I., and Z. Liu, 2000: Response of the equatorial thermocline to extratropical buoyancy forcing. *J. Phys. Oceanogr.*, **30**, 2883–2905.
- Sohn, B.-J., H.-S. Chung, D.-H. Kim, D. Perkey, F. R. Robertson, and E. A. Smith, 2001: Use of satellite-derived water vapor data to investigate northwestward expansion of North Pacific subtropical high during 1995 summer. *J. Meteor. Soc. Japan*, **79**, 1059–1075.
- Sun, D.-Z., and R. S. Lindzen, 1993: Distribution of tropical tropospheric water vapor. *J. Atmos. Sci.*, **50**, 1643–1660.
- Sun, D.-Z., and A. H. Oort, 1995: Humidity-temperature relationships in the tropical troposphere. *J. Climate*, **8**, 1974–1987.
- Sun, D.-Z., T. Zhang, and S.-I. Shin, 2004: The effect of subtropical cooling on the amplitude of ENSO: A numerical study. *J. Climate*, **17**, 3789–3798.
- Tanimoto, Y., H. Nakamura, T. Kagimoto, and S. Yamane, 2003: An active role of extratropical sea surface temperature anomalies in determining anomalous turbulent heat flux. *J. Geophys. Res.*, **108**, 3304, doi:10.1029/2002JC001750.
- Tanimoto, Y., and S. P. Xie, 2002: Inter-hemisphere decadal variations in SST, surface wind, heat flux and cloud cover over the Atlantic Ocean. *J. Meteor. Soc. Japan*, **80**, 1199–1219.
- Trenberth, K. E., G. W. Branstator, D. Karoly, A. Kumar, N. C. Lau, and C. Ropelewski, 1998: Progress during TOGA in understanding and modeling global teleconnections associated with tropical sea surface temperatures. *J. Geophys. Res.*, **103**, 14 291–14 324.
- Trenberth, K. E., and C. J. Guillemot, 1995: Evaluation of the global atmospheric moisture budget as seen from analyses. *J. Climate*, **8**, 2255–2272.
- Trenberth, K. E., and C. J. Guillemot, 1998: Evaluation

- of the atmospheric moisture and hydrological cycle in the ncep/ncar reanalysis. *Clim. Dyn.*, **14**, 213–231.
- Wallace, J. M., E. M. Rasmusson, T. P. Mitchell, V. E. Kousky, E. S. Sarachik, and H. V. Storch, 1998: On the structure and evolution of ENSO-related climate variability in the tropical Pacific: Lessons from TOGA. *J. Geophys. Res.*, **103**, 14 241–14 259.
- Wang, B., R. Wu, and X. Fu, 2000: Pacific-east Asian teleconnection: How does ENSO affect east Asian climate? *J. Climate*, **13**, 1517–1536.
- Wang, B., and Q. Zhang, 2002: Pacific-East Asian teleconnection, part II: How the Philippine Sea anticyclone established during development of El Niño. *J. Climate*, **15**, 3252–3265.
- Wang, C., 2002: Atmospheric circulation cells associated with the El Niño-Southern oscillation. *J. Climate*, **15**, 399–419.
- Weng, S.-P., 2009: Propagating coupled modes between the tropical indo-pacific ocean heat content and sst anomalies in the interannual timescale. *J. Meteor. Soc. Japan*, **87** (2), 307–333, doi:10.2151/jmsj.87.307.
- Woodruff, S. D., R. J. Slutz, R. L. Jenne, and P. M. Steurer, 1987: A comprehensive ocean-atmosphere data set. *Bull. Amer. Meteorol. Soc.*, **68**, 1239–1250.
- Xie, S. P., Y. Tanimoto, H. Noguchi, and T. Matsuno, 1999: How and why climate variability differs between the tropical Atlantic and Pacific. *Geophys. Res. Lett.*, **26**, 1609–1612.
- Yoneyama, K., 2003: Moisture variability over the tropical western Pacific ocean. *J. Meteor. Soc. Japan*, **81**, 317–337.